Construction and Building Materials 495 (2025) 143655

Contents lists available at ScienceDirect

Construction and Building Materials

journal homepage: www.elsevier.com/locate/conbuildmat

Enhanced asphalt fume suppression through cellulose- and lignin-rich biochar: A structure-property relationship

Hao Duan [a], Quantao Liu [a], Yanheng He [a], Zizhou Shen [a], Xiaobin Han [b], Shi Xu [c,d], Jianying Yu [a,*]

[a] State Key Laboratory of Silicate Materials for Architectures, Wuhan University of Technology, Wuhan 430070, PR China
[b] School of Electric Power, Civil Engineering and Architecture, Shanxi University, Taiyuan 030031, PR China
[c] School of Civil Engineering and Architecture, Wuhan University of Technology, Luoshi Road 122, Wuhan 430070, PR China
[d] Faculty of Civil Engineering and Geosciences, Delft University of Technology, Stevinweg 1, 2628 CN, Delft, the Netherlands

ARTICLE INFO

Keywords:
Biochar
Asphalt fume
Structure
Adsorption
VOCs

ABSTRACT

Despite biochar has a good ability in suppressing asphalt fumes, the relationship between the structure of biochar derived from different plant sources and its performance in adsorbing fumes has not yet been explored. In this study, biochar with varying structures and compositions was prepared from cellulose-rich (tea stalks and poplar sawdust) and lignin-rich (coconut shell fiber and loofah sponge) biomass and used as asphalt fume suppressants. Structural characterization revealed that all biochar developed abundant pore structures. Specifically, cellulose-rich biochar featured macro-/mesoporous structures with relatively oxygen-rich surfaces, while lignin-rich biochar exhibited micro-/mesoporous structures with enhanced π-conjugated graphitic frameworks. Asphalt fume adsorption tests showed that, cellulose-based biochar was more effective in adsorbing H_2S and NO_x, whereas lignin-rich biochar exhibited superior adsorption of VOCs. GC-MS analysis confirmed that cellulose-rich biochar facilitates the adsorption of polar pollutants due to its higher oxygen-rich surfaces, while lignin-rich biochar enhances the adsorption of aromatic pollutants through π–π interactions. Physical property tests of asphalt showed that the macropores of cellulose-rich biochar absorbed more light fractions and promoted an increase in asphaltenes content, significantly enhancing high-temperature performance but having an adverse effect on asphalt ductility.

1. Introduction

Asphalt pavement are widely used due to their comfortable driving conditions and easy maintenance [1–3]. However, during high-temperature construction, asphalt releases hazardous fumes containing volatile organic compounds (VOCs) [4], hydrogen sulfide (H_2S), sulfur oxides (SO_2, and nitrogen oxides (NO_2) [5,6]. Studies have shown that the concentration of VOCs released from heated asphalt exceeds 800 ppm, while the concentration of H_2S surpasses 200 ppm, posing serious health risks to construction workers [7]. Additionally, these pollutants lead to the formation of secondary organic aerosols and fine particulate matter (PM2.5), exacerbating air pollution [8,9]. Therefore, developing efficient and sustainable asphalt fume control technologies has become a key issue that urgently needs to be addressed in the fields of road engineering and environmental management.

Currently, the primary method for reducing asphalt fumes is additive based technology. Conventional additives, such as activated carbon, layered silicate materials, and zeolites, have been shown to effectively inhibit the emission of VOCs, but they have certain limitations. For example, activated carbon [10] and montmorillonite [11,12] adsorb asphalt VOCs through their pore or layered structures; however, they exhibit poor dispersion in asphalt, and their fume suppression effect is highly dependent on dosage (>5 % of asphalt mass), which severely compromises the low-temperature and rheological properties of asphalt. Zeolite [13,14] exhibited a relatively low adsorption capacity for asphalt fumes, resulting in limited effectiveness in suppressing asphalt VOCs, with a maximum reduction of 37 % in total VOC emissions. While metal-organic framework (MOF) [15] materials can achieve a 50.4 % reduction in VOC emissions at a low dosage (0.6 %), their high cost and complex preparation process hinder large-scale production and application. Therefore, the development of more efficient, environmentally friendly materials that combine fume suppression with practicality has

* Corresponding author.
E-mail address: jyyu@whut.edu.cn (J. Yu).

https://doi.org/10.1016/j.conbuildmat.2025.143655
Received 12 May 2025; Received in revised form 24 August 2025; Accepted 13 September 2025
Available online 17 September 2025

become a research focus.

Biochar is a porous material produced through the pyrolysis of biomass under oxygen-limited conditions [16,17]. The production of biochar typically involves three main stages: (i) pretreatment and drying of the raw biomass to remove excess moisture and improve thermal efficiency; (ii) pyrolysis under oxygen-limited conditions, during which cellulose, hemicellulose, and lignin decompose to form volatile products and a stable carbon-rich solid; and (iii) stabilization or activation of the resulting char, which may include cooling under inert conditions or post-treatment to enhance porosity and surface reactivity [18]. These stages not only determine the yield of biochar but also strongly influence its pore structure, surface functional groups, and overall adsorption performance. Previous studies have demonstrated that the incorporation of biochar into asphalt can effectively modify its fundamental properties. Yegane et al. [19] reported that the rough and porous structure of biochar significantly enhanced the high-temperature performance and rutting resistance of asphalt, while simultaneously improving its fatigue life. Celauro et al. [20] showed that biochar increased the stiffness of asphalt without compromising its workability or processability. Rajib et al. [21] further revealed that the ultraviolet shielding and free-radical scavenging abilities of biochar helped maintain the colloidal balance of asphalt during aging, thereby markedly improving its anti-aging performance. Collectively, these findings establish biochar as a feasible asphalt modifier and provide a solid foundation for exploring its additional functionalities. Building upon this applicability, recent research has shifted attention toward the pollutant adsorption capacity of biochar. Owing to its high porosity, large specific surface area, excellent stability, and strong adsorption capacity, biochar exhibits superior performance in various environmental applications, such as soil improvement [22], wastewater remediation [23], and the reduction of pollutant emissions [24]. Recognizing these advantages, researchers have recently explored its application in asphalt fume treatment, and have demonstrated its effectiveness in VOCs adsorption. Mousavi et al. [25] investigated the effects of different biochar (peanut shell, Douglas fir, pine bark, etc.) on asphalt fume emissions. The results showed that pine bark biochar exhibited the most significant inhibition of aromatic VOCs, peanut shell biochar was highly effective against alkene VOCs, and Douglas fir biochar had the strongest effect on alkane VOCs. Zhou et al. [26] compared the inhibitory effects of rice husk and rice straw biochar on asphalt VOCs. While rice husk biochar effectively suppressed the release of VOCs, rice straw biochar unexpectedly promoted the emission of VOCs. Although previous studies have confirmed the potential of biochar in reducing asphalt fume emissions, they also reveal significant variations in adsorption performance depending on the biomass precursor. However, the fundamental mechanisms behind these differences, particularly how biomass composition affects the pore structure, surface chemistry, and fume adsorption behavior of biochar, remain unclear. Therefore, elucidating these mechanisms is crucial for optimizing biochar selection and maximizing its efficiency in asphalt fume treatment.

Plant biomass is primarily composed of cellulose, hemicellulose, and lignin [27]. Hemicellulose is an amorphous polysaccharide made up of sugar units like xylan and mannose, whereas cellulose is made up of aliphatic chains created by the linear bonding of D-glucose units, and lignin is considered a three-dimensional aromatic polymer composed of phenylpropane units [28]. Due to the significant differences in the composition of different biomass sources, the resulting biochar exhibits corresponding differences in composition and structure, ultimately affecting its adsorption performance.

In this study, four types of biomass feedstocks (tea stalk, poplar sawdust, coconut shell fiber, and loofah sponge) were selected for biochar preparation. The rationale for their selection is threefold. First, these materials are abundant agricultural and forestry byproducts, offering low cost and wide availability while contributing to resource recycling and waste reduction. Second, they are representative of distinct lignocellulosic compositions: tea stalk and poplar sawdust are relatively rich in lignin, whereas coconut shell fiber and loofah sponge are predominantly cellulose-rich. This distinction provides an opportunity to systematically investigate how biomass composition governs the pore structure, surface chemistry, and pollutant adsorption performance of biochar. Third, these feedstocks have previously been investigated as adsorbents in various environmental applications, demonstrating their potential suitability. For example, coconut shell biochar has been applied in remove pesticide residues or fluoride ions from wastewater [29,30], while loofah sponge biochar has shown effectiveness in the adsorption of organic pollutants [31,32]. Similarly, tea stalk and poplar sawdust biochars have been reported to wastewater treatment or capture gaseous pollutants [33–35].

Despite the proven potential of biochar in asphalt fume control, previous studies have primarily focused on specific biomass types and single-pollutant adsorption, lacking mechanistic insight into how biomass composition governs biochar structure and pollutant interactions. In reality, asphalt fumes comprise a complex mixture of gaseous pollutants, and the suppression efficiency of different types of biochar varies considerably depending on the physicochemical properties of these pollutants. To bridge this gap, this study systematically investigates the influence of biomass components (cellulose and lignin) on the structural evolution of biochar and its multi-pollutant adsorption behavior. To achieve this, four biomass feedstocks were selected based on their varying cellulose, hemicellulose, and lignin contents.

To this end, the pore characteristics, microstructure, elemental, and functional group properties of the prepared biochar were characterized using scanning electron microscopy (SEM), Brunauer-Emmett-Teller (BET) analysis, elemental analysis (EA), and Fourier-transform infrared spectroscopy (FTIR), respectively. A photoionization detector (PID) was used to evaluate their inhibitory effects on VOC, hydrogen sulfide, nitrogen oxides, and sulfur dioxide concentrations in asphalt fumes. Thermal desorption gas chromatography mass spectrometry (TD-GC-MS) was employed to provide a detailed characterization of VOCs composition and concentrations of asphalt binders with different biochar. In addition, the effects of biochar incorporation on the SARA fractions and physical properties of asphalt were also evaluated. The experimental design and tests are illustrated in Fig. 1.

2. Materials and methods

2.1. Materials

This study utilized penetration grade 70 asphalt provided by Research Institute of Petro China Fuel Oil Co., Ltd., with performance requirements outlined in Table 1. The biochar was derived from four biomass materials (tea stalks, poplar sawdust, coconut shell fiber, and loofah sponge.), as shown in Fig. 2.

The proportions of cellulose, hemicellulose and lignin of the four biomasses are shown in Table 2. Since hemicellulose generally decomposes during pyrolysis and contributes little to the formation of solid biochar, this paper primarily focuses on the contents of cellulose and lignin. As shown in the table, tea stalks and poplar sawdust have higher lignin content, which are called lignin-rich biomass. The contents of cellulose in the components of coconut shell and loofah sponge are higher. Similarly, they are called cellulosic-rich biomass.

2.2. Preparation of biochar

The biochar production process consists of three sequential stages: feedstock pretreatment, oxygen-limited pyrolysis, and post-processing.

Feedstock pretreatment: Four types of biomasses (tea stalks, poplar sawdust, coconut shell fiber, and loofah sponge) were crushed using a crusher operated at 3000 rpm for 15 min. The comminuted biomass was then sieved through 200-mesh screens.

Oxygen-limited pyrolysis: Following the method of Wei [36], the prepared biomass samples were compacted in alumina crucibles (50 mm

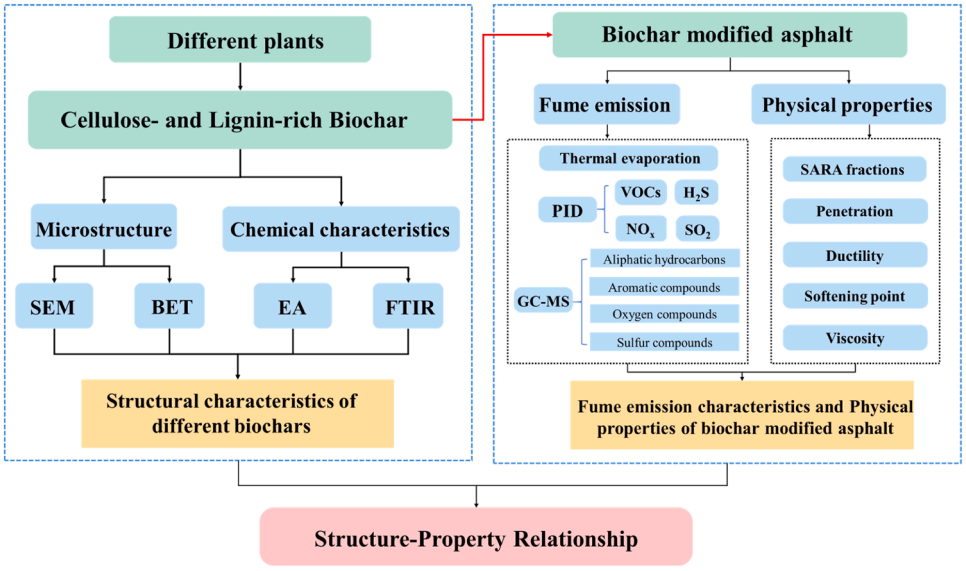

Fig. 1. Research flowchart.

Table 1
Physical properties of asphalt.

Item	Test value	Test standard
Penetration (25℃, 0.1 mm)	77	ASTM D 5
Softening point (℃)	48.3	ASTM D 36
Viscosity (60℃, Pa·s)	205	ASTM D 4402
Ductility (15℃, cm)	60	ASTM D 113
Flash point (℃)	251	ASTM D 92
Density (g/cm^3)	1.084	ASTM D 70
Retained penetration ratio (%)	72	ASTM D 5

diameter × 30 mm height) and hermetically sealed with double-layer aluminum foil packaging to establish oxygen-limited conditions. The wrapped crucibles were then placed in a muffle furnace, where the heating protocol involved increasing the temperature to 500℃ at a rate of 15℃/min and maintaining it for 2 h. The preparation process of biochar is shown in Fig. 3. Based on our previous research [37], a pyrolysis temperature of 500℃ was selected because it provides a favorable balance between biochar yield, pore development, and the preservation of oxygen-containing functional groups. Lower temperatures (<400℃) often lead to incomplete pyrolysis and insufficient pore formation, while higher temperatures (>600℃) may cause excessive loss of surface functionalities that are important for pollutant

Table 2
Cellulose, hemicellulose and lignin of four biomass.

Item	Cellulose/%	Hemicellulose/%	Lignin/%
Tea stalk	28	11	61
Poplar sawdust	24	28	48
Coconut shell fiber	60	6	34
Loofah sponge	73	9	18

Fig. 2. Four types of biomass raw materials: (a) tea stalk; (b) poplar sawdust; (c) coconut shell fiber; (d) loofah sponge.

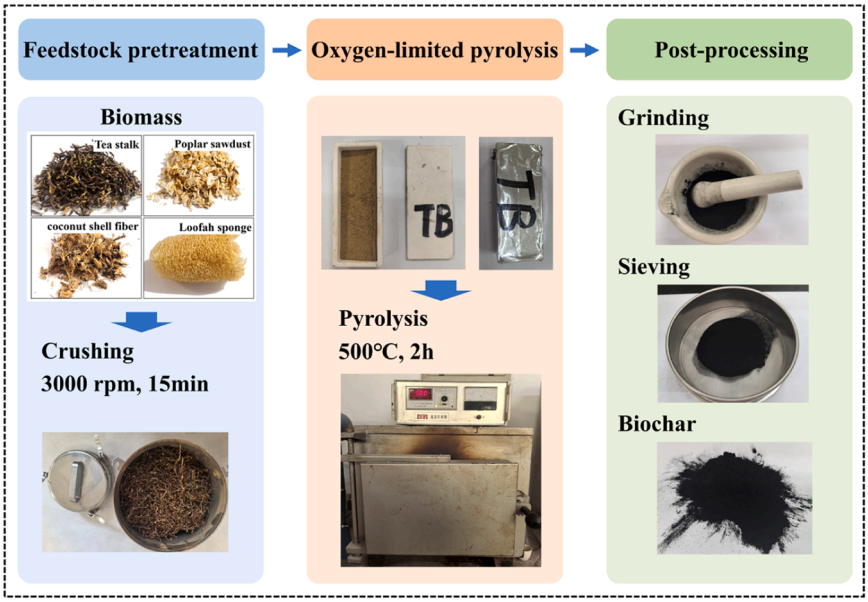

Fig. 3. Preparation process of biochar.

adsorption. Therefore, 500℃ was considered an optimal compromise for preparing biochar with both well-developed structure and active surface chemistry.

Post-processing: After being cooled to room temperature in a desiccator, the obtained biochar was removed, ground, and screened through a 200-mesh sieve. The biochar prepared from tea stalk, poplar sawdust, coconut shell fiber, and loofah sponge were labeled as TB, PB, CB and LB respectively.

2.3. Preparation of biochar-modified asphalt

Biochar-modified asphalt was prepared using the melt blending method. First, the asphalt was heated to 140℃, and biochar was added at concentrations of 0.25 %, 0.5 %, 1 %, and 2 % by weight of the asphalt. The mixture was then stirred at 2000 rpm for 45 min to ensure uniform dispersion, resulting in the formation of biochar-modified asphalt. The samples of biochar-modified asphalt were labeled as XTBA, XPBA, XLBA, and XCBA, where "X" indicates the percentage of biochar content in the asphalt. For clarity, the composition and corresponding abbreviations of biochar-modified asphalt are presented in Table 3.

2.4. Characterizations of biochar

2.4.1. BET

The BET surface area of the biochar samples was determined using nitrogen adsorption-desorption isotherms. Prior to analysis, all samples were degassed at 150℃ under vacuum for 12 h to remove moisture and adsorbed gases. The micropore volume (pores < 2.0 nm in diameter) and the corresponding surface area were calculated using the T-plot method. The T-plot is a statistical thickness analysis of nitrogen adsorption isotherms that distinguishes between micropore and mesopore contributions, allowing separate evaluation of micropore volume and external surface area. This method has been widely recommended for porous materials characterization by the IUPAC report. To estimate the total pore volume of each biochar sample, the adsorbed quantity (g) was converted into liquid nitrogen volume based on a density of 0.808 g/mL at atmospheric pressure near saturation. The average pore diameter of each biochar sample was then calculated using Eq. 1:

$$\text{Average pore diameter} = \frac{4 \times V_t}{S_{BET}} \quad (1)$$

Where:
V_t represents the total pore volume
S_{BET} denotes the BET surface area

Table 3
Composition and abbreviation of biochar modified asphalt.

Biomass source	Biochar abbreviation	Asphalt sample abbreviation	Biochar content (% by asphalt weight)
Tea stalk	TB	XTBA	0.25, 0.5, 1, 2
Poplar sawdust	PB	XPBA	0.25, 0.5, 1, 2
Coconut shell fiber	CB	XCBA	0.25, 0.5, 1, 2
Loofah sponge	LB	XLBA	0.25, 0.5, 1, 2

2.4.2. SEM

The morphology and structure of the biochar were analyzed using a scanning electron microscope (FEG450, FEI Company, USA). Prior to imaging, the biochar sample was coated with a thin layer of gold through sputtering for 30 s to improve conductivity. The prepared sample was then placed on the test plate and secured with conductive adhesive for analysis.

2.4.3. Elemental analysis

The elemental analyzer (Vario EL cube, Germany) was used to measure the carbon, hydrogen, nitrogen, and sulfur content of the biochar. The principle of analysis was dynamic adsorption-procedural desorption-TCD detection. The content of the oxygen element was obtained using the subtraction method: O%= 100 % - (C + H + N + S + ash, %). The ash content, representing the number of inorganic substances, was determined by heating the biochar samples in a muffle furnace at 750℃ for 6 h.

2.4.4. FTIR

FTIR is a commonly used spectroscopic technique that provides information about molecular structure and chemical bonds by measuring the absorption of different infrared wavelengths. The FTIR spectra of the biochar were obtained using the potassium bromide pellet method. First, 2.0 mg of the sample was ground in a mortar. Then, 100–200 mg of finely ground KBr was added and thoroughly mixed. Finally, the mixture

was placed in a compression mold to form a transparent pellet suitable for testing with an FTIR spectrometer (Frontier, PerkinElmer, USA). The characteristic absorption peaks of the biochar were analyzed in the wavenumber range of 400–4000 cm^{-1} , with 32 scans per sample and a resolution of 4 cm^{-1} .

2.5. Characterization of biochar-modified asphalt

2.5.1. Thermal evaporation loss

The evaluation of fume emissions during asphalt heating was conducted by measuring the mass loss of asphalt specimens during the Thin Film Oven Test (TFOT) aging process, in accordance with ASTM D1754. The test procedure is as follows: Precisely weigh 50 g ± 0.5 g of asphalt into a flat-bottomed metal container with a diameter of 55 mm, then heat it in an oven at 163 ℃ for 5 h. The mass variation of the asphalt is recorded throughout this process. Each sample is tested three times, and the average value is taken as the final test result.

2.5.2. Concentration of various components in asphalt fume

Asphalt fumes primarily consist of volatile organic compounds (VOCs), nitrogen oxides (NO_x), sulfur dioxide (SO_2, and hydrogen sulfide (H_2S). In this study, the main components of asphalt fumes were analyzed. A photoionization detector (PID; Korno GT-1000, China) was employed in a four-channel detection mode to measure the concentrations of VOCs, H_2S, NO_x, and SO_2. The detection ranges for the gases were as follows: VOCs: 0–2000 ppm, H_2S: 0–200 ppm, SO_2: 0–100 ppm, and NO_x: 0–500 ppm, with a resolution of 0.1 ppm for each measurement.

The asphalt fume content was determined according to the procedure illustrated in Fig. 4. In brief, 200 g of asphalt was placed in a three-neck flask and heated in an oil bath at 160℃, with stirring maintained at 300 rpm for 1 h. The fumes generated during this process were drawn by a gas pump into a collection bottle immersed in a 5℃-water bath for condensation. The condensed fumes were then analyzed using a PID detector for 3 min, and the maximum value recorded during this period was taken. Each sample was tested in triplicate, and the average value was reported.

2.5.3. Analysis of VOCs components in asphalt fume

Volatile organic compounds (VOCs) in asphalt fumes comprise a complex mixture of non-methane hydrocarbons (C5-C20 alkanes, alkenes, alkynes, and aromatics), oxygenated derivatives (aldehydes, ketones, alcohols), and heteroatomic compounds (halogenated/nitrogenated/sulfur-containing species). To investigate the component-specific suppression effects of biochar, Thermal desorption gas chromatography mass spectrometry (TD-GC-MS; Agilent 7890B-5977B, USA) was used to analyze the composition of asphalt fume, following widely reported methods in the literature [6,38]. The procedure for collecting fume is as follows: (1) The asphalt (50 ± 0.05 g) were loaded into a nitrogen-purged three-neck flask and equilibrated at 160 ± 2℃ for 30 min using a digital hotplate. (2) A calibrated air sampling pump (SKC 222–1001) drew fumes through an adsorption column (Agilent 222–5532LTM) at 500 mL/min for 10 sec, achieving a total sampled volume of 83.3 mL. (3) Loaded sorbent tubes were immediately sealed with PTFE caps and stored at 4℃ in amber vials prior to analysis. After the fume collection is completed, the adsorption column is inserted into a GC-MS system for the analysis of the collected gas components.

2.5.4. Asphalt SARA fractions test

According to the differences in polarity among the components of asphalt, it can be separated into four components: saturated hydrocarbons, aromatic hydrocarbons, resins, and asphaltenes, collectively known as the SARA components of asphalt. In this study, the SARA composition of biochar-modified asphalt was measured according to ASTM D4214–2001. All samples were tested three times and the average value was taken as the final result.

2.5.5. Physical properties test

The penetration, softening point, 15℃ ductility, and 60℃ viscosity of the biochar-modified asphalt were tested according to ASTM D 5, ASTM D 36, ASTM D 113, and ASTM D 2171, respectively. All performance tests were repeated three times, with the test results being the average of the three outcomes and the error bars representing the standard deviation of the three tests.

3. Results and discussion

3.1. Characterizations of biochar

3.1.1. Pore characteristics

Fig. 5 presents the nitrogen adsorption isotherms of the four biochar samples, all of which exhibit Type IV isotherm characteristics, according to the IUPAC classification. This isotherm type is typically associated with mesoporous materials. Three distinct adsorption stages are observed: (1) The gradual rise in the low-pressure region ($P/P_0 \leq 0.1$) corresponds to monolayer adsorption on the pore walls; (2) The

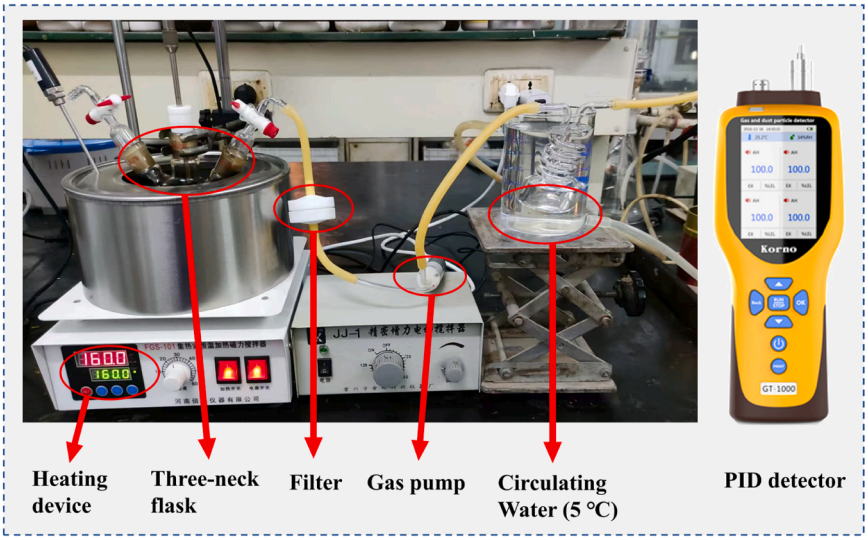

Fig. 4. Testing process for asphalt fume.

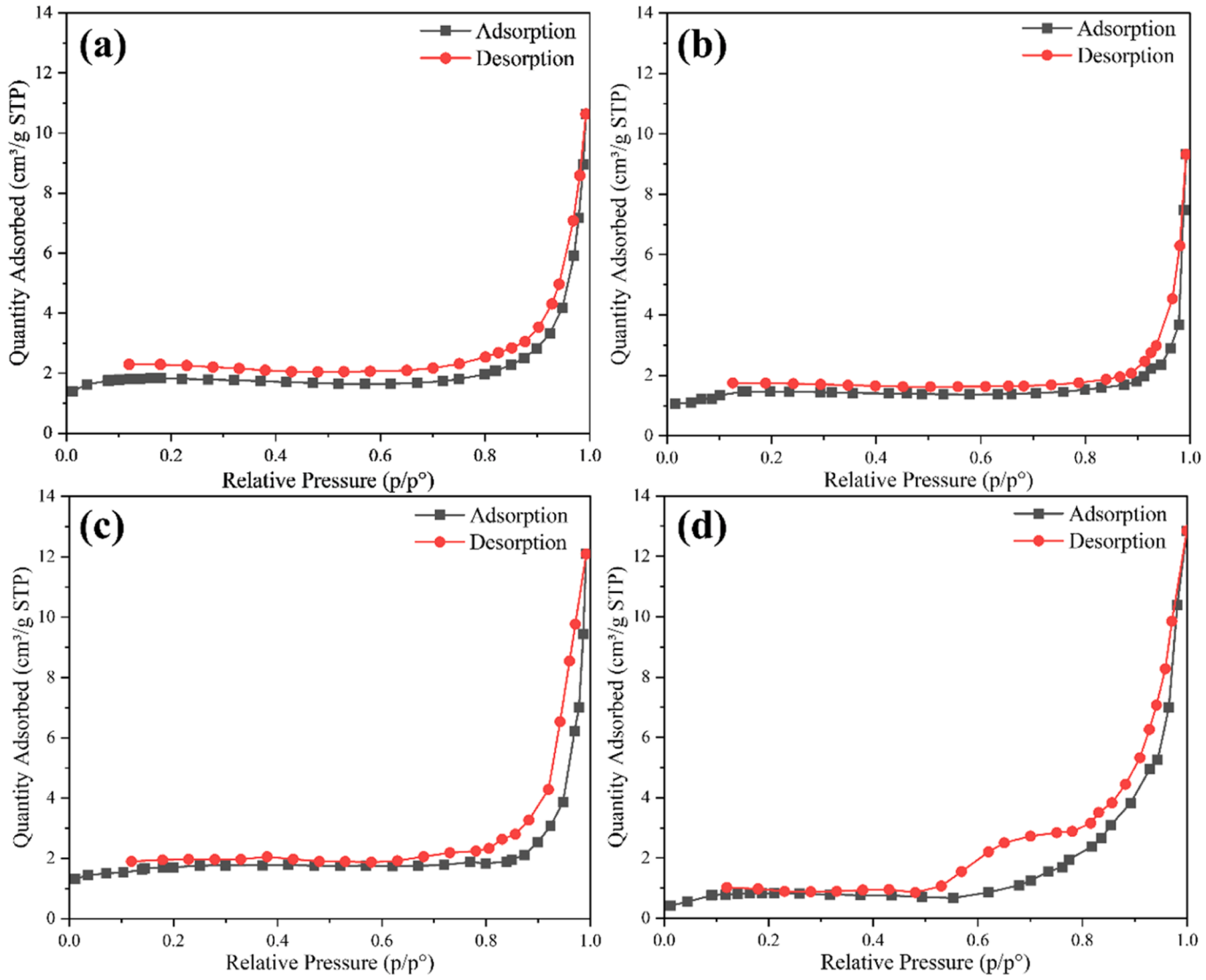

Fig. 5. Nitrogen adsorption-desorption curves of biochar derived from different biomass: (a) TB; (b) PB; (c) CB; (d) LB.

adsorption plateau in the middle-pressure region (0.1–0.9) represents the transition to multilayer adsorption; (3) The steep increase in the high-pressure region ($P/P_o > 0.9$) indicates capillary condensation occurring within macropores.

The nitrogen adsorption isotherm of TB (Fig. 5a) exhibited a steep initial increase at low relative pressure, indicating a well-developed microporous structure. As the relative pressure increased, a distinct hysteresis loop in the desorption branch suggested the coexistence of mesopores and macropores, likely formed due to partial pore collapse during pyrolysis. This hierarchical pore system is consistent with lignin-rich precursors, which tend to undergo cross-linking and aromatic condensation, favoring the formation of micropores [39]. Compared to TB, PB (Fig. 5b) demonstrated a similar isotherm profile but with a lower adsorption capacity and a less pronounced slope in the low-pressure region, suggesting a lower micropore volume. This suggests a smaller micropore volume and less efficient pore development, probably due to subtle differences in precursor composition and thermal degradation pathways.

In contrast, the cellulose-rich biochar CB and LB (Figs. 5c and 5d) showed a slower adsorption rise at low pressures, indicated of lower specific surface areas and limited microporosity. Their nearly overlapping adsorption/desorption branches in this region confirmed that micropores contributed minimally to adsorption. However, the obvious hysteresis loop in the medium to high pressure region indicates that it had more mesopores and macropores. This behavior reflects the decomposition mechanism of cellulose, which generates volatiles that expand the structure and create large voids, while restricting micropore development. Further comparison of hysteresis loop characteristics reveals notable differences in pore heterogeneity. Lignin-rich biochar (TB and PB) exhibited H4-type hysteresis loops within the $P/P_o = 0.45–0.85$ range, indicative of slit-like mesopores. By contrast, CB and LB exhibited a two-stage pattern: near-complete overlap of adsorption/desorption at low pressures (monolayer adsorption) and an H3-type hysteresis at high pressures, characteristic of plate-like particle aggregates with macropores. These observations underscore the critical role of biomass composition and pyrolysis conditions in shaping the pore architecture, with lignin-rich biochar promoting microporosity and cellulose-derived biochar favoring a macropore-dominated structure.

The pore size distribution curves of the four types of biochar, as shown in Fig. 6(a–d), reveal distinct structural differences associated with their feedstock origins. The lignin-rich biochar TB and PB (Figs. 6a and 6b), exhibited a predominant distribution of pores within the sub-20 nm range, indicating that micropores and mesopores dominate their porous architecture. The sharp decline in pore volume with increasing pore size suggests a relatively low abundance of macropores. This trend was characteristic of biochar formed through the condensation and

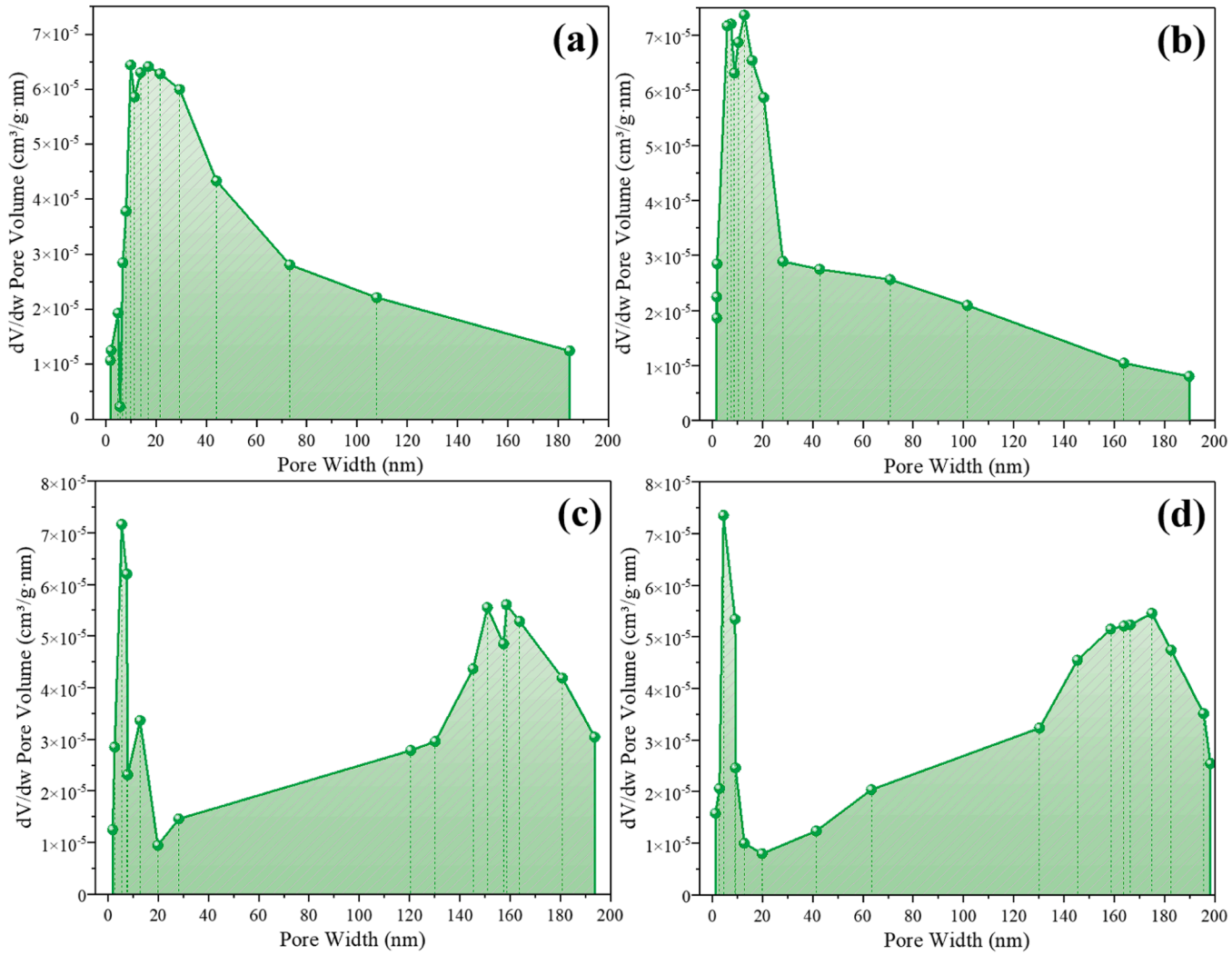

Fig. 6. Pore size distribution of biochar derived from different biomass: (a)TB; (b)PB; (c)CB; (d)LB.

cross-linking of lignin-rich precursors, which favor micropore development due to their aromatic carbon content and thermal stability. In contrast, the cellulose-rich biochar, CB and LB (Figs. 6c and 6d), exhibited a bimodal pore size distribution, with one peak below 20 nm and another around 160 nm. This indicated the coexistence of both mesopores and well-developed macropores. The presence of macropores can be attributed to the inherent cellular structure of biomass and the partial collapse of pore walls during pyrolysis. The differences in pore structure between lignin- and cellulose-rich biochar suggest that feedstock composition significantly influences the pore formation mechanism, with lignin favoring micropore-rich structures and cellulose yielding materials with greater macropores.

Quantitative results in Table 4 confirm these trends. TB and PB exhibited higher specific surface areas but smaller average pore diameters, consistent with their micropores and mesopores dominated structure. In contrast, CB and LB displayed lower specific surface areas and larger average pore diameters, consistent with their pronounced macropores. Micropores formation is primarily driven by carbon loss and the contraction of the carbon skeleton during pyrolysis, whereas macropores often originate from the natural honeycomb-like structure of biomass. Since surface area correlates positively with micropore fraction, the higher adsorption potential of lignin-derived biochar can be attributed to its microporosity, whereas cellulose-derived biochar provides large macropores that may enhance mass transfer but contribute less to surface area.

Table 4
BET analysis results of biochar derived from different biomass.

	TB	PB	CB	LB
BET Surface Area (m^2/g)	6.93	5.88	2.49	1.75
Average pore diameter (nm)	8.78	11.17	62.14	87.99

3.1.2. *Microstructure*

The SEM images in Fig. 7 reveal distinct microstructural variations among the four types of biochar, highlighting the influence of feedstock composition on pore morphology and particle aggregation. These differences can be attributed to both the inherent structural characteristics of the precursor biomass and the varying thermal decomposition behaviors of cellulose, hemicellulose, and lignin during pyrolysis at 500°C. The decomposition dynamics of these components significantly affect the distribution and properties of the resulting pyrolysis products.

The lignin-rich biochar (Figs. 7a and 7b) retained relatively intact skeletal structures, with irregularly shaped particles and fibrous networks. Their surfaces feature heterogeneously distributed pores, contributing to increased surface roughness and textural complexity. Notably, the biochar in Fig. 7a presented a more porous structure with finer fragmented particles, whereas the biochar in Fig. 7b showed greater aggregation with larger, denser fragments. These characteristics are consistent with the high thermal stability of lignin, which tends to

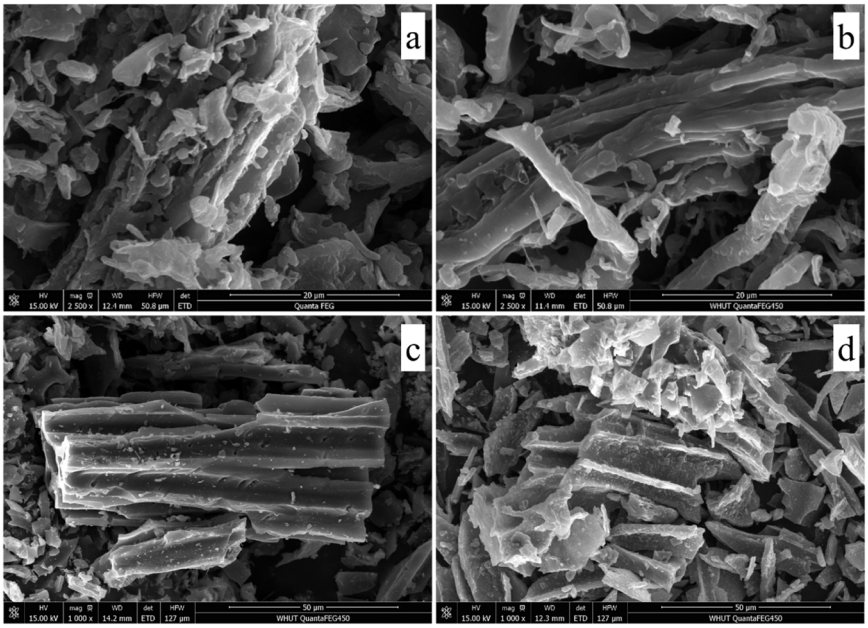

Fig. 7. SEM images of different biochar derived from different biomass: (a)TB; (b)PB; (c)CB; (d)LB.

undergo condensation and cross-linking reactions. Such processes stabilize the carbon matrix and promote the formation of micropores within a rigid carbon framework. In contrast, the cellulose-rich biochar (Figs. 7c and 7d) exhibits highly degraded structures due to the lower thermal stability of cellulose. The SEM images reveal residual fibrous frameworks interspersed with thin, flake-like fragments, indicating more extensive material decomposition. Structural differences were also evident between CB and LB: the former displays smoother surfaces with a moderate number of visible pores, while the latter exhibits pronounced folds and an irregular, wrinkled morphology. These characteristics can be linked to the rapid release of volatiles during cellulose pyrolysis, which generates interconnected macropores while retaining aspects of the original cellular architecture.

Overall, the SEM observations indicate that lignin-rich biochars favor micropore development through structural condensation, while cellulose-derived biochars produce macropore-rich networks due to volatile-driven expansion and framework collapse. This structural dichotomy is significant: micropores contribute to higher specific surface areas and enhanced adsorption of small molecules, whereas macropores facilitate mass transport and fume diffusion. Thus, the balance between lignin and cellulose in the precursor biomass directly governs both the pore architecture and the potential fume adsorption performance of the resulting biochar.

3.1.3. Element analysis

The biochar yield and ash content derived from different biomass materials (Fig. 8a–b) exhibited notable variations, reflecting the compositional differences among feedstocks. The lignin-rich biochar TB and PB, demonstrated the highest yields, whereas cellulose-rich biochar CB and LB produced lower biochar quantities. Similarly, CB and LB exhibited significantly higher ash contents than PB and TB. This variation can be explained by the thermal degradation behavior of biomass constituents: cellulose and hemicellulose decompose mainly within 200–400 °C, releasing large amounts of volatiles, whereas lignin degrades more gradually across 400–600 °C due to its aromatic and cross-linked structure. Ash content displayed an opposite trend, with CB and LB containing significantly higher amounts than PB and TB. This can be linked not only to the mineral composition of the biomass but also to environmental factors. In particular, CB, derived from coconut shells grown in coastal regions, likely accumulated salts and inorganic minerals from seawater, which persisted after pyrolysis and contributed to its elevated ash content. Such ash enrichment is consistent with observations in other agricultural residues exposed to saline environments.

The elemental composition and H/C and O/C mass ratios of the biochar (Fig. 8c–d) further illustrate the differences arising from feedstock variation. Biochar derived from lignin-rich biomass exhibited higher carbon and hydrogen content but lower oxygen content compared to those produced from cellulose-rich precursors. This trend arises because cellulose pyrolysis generates a greater proportion of oxygenated organic volatiles, which deposit on the biochar surface, increasing oxygen content and reducing carbon concentration. The pyrolytic transformation of biomass involves the progressive loss of hydrogen and oxygen through dehydration and decarboxylation reactions, leading to structural reorganization and increased aromaticity [40]. These changes can be effectively represented using Van Krevelen plots (Fig. 8d), where the H/C and O/C mass ratios serve as indicators of biochar's degree of carbonization and aromatic condensation. As shown in the results, CB and LB exhibited higher H/C and O/C ratios compared to TB and PB, consistent with their higher oxygen and hydrogen content but lower carbon concentration. This finding supports the well-established observation that lignin-derived biochar favors the formation of stable polyaromatic structures, whereas cellulose-rich feedstocks tend to retain more oxygen-functionalized groups. These structural differences significantly influence the physicochemical properties of biochar, particularly in applications related to adsorption, catalysis, and soil amendment, where surface chemistry and porosity play critical roles.

3.1.4. Functional group analysis

The functional group composition of the biochar was analyzed using FTIR, and the corresponding spectra are presented in Fig. 9. Due to the high degree of carbonization, the biochar exhibited broadly similar absorption features; however, distinct differences in specific functional groups remain evident. A broad absorption band at 3434 cm^{-1} corresponds to the stretching vibrations of hydroxyl (-OH) groups, which are typically associated with surface-bound water and hydrogen-bonded hydroxyl functionalities. The relatively weak absorption peaks at 2909 cm^{-1} and 2852 cm^{-1} , assigned to methyl ($-CH_3$) and methylene ($-CH_2-$) stretching vibrations, indicate significant degradation of aliphatic structures due to molecular chain cleavage

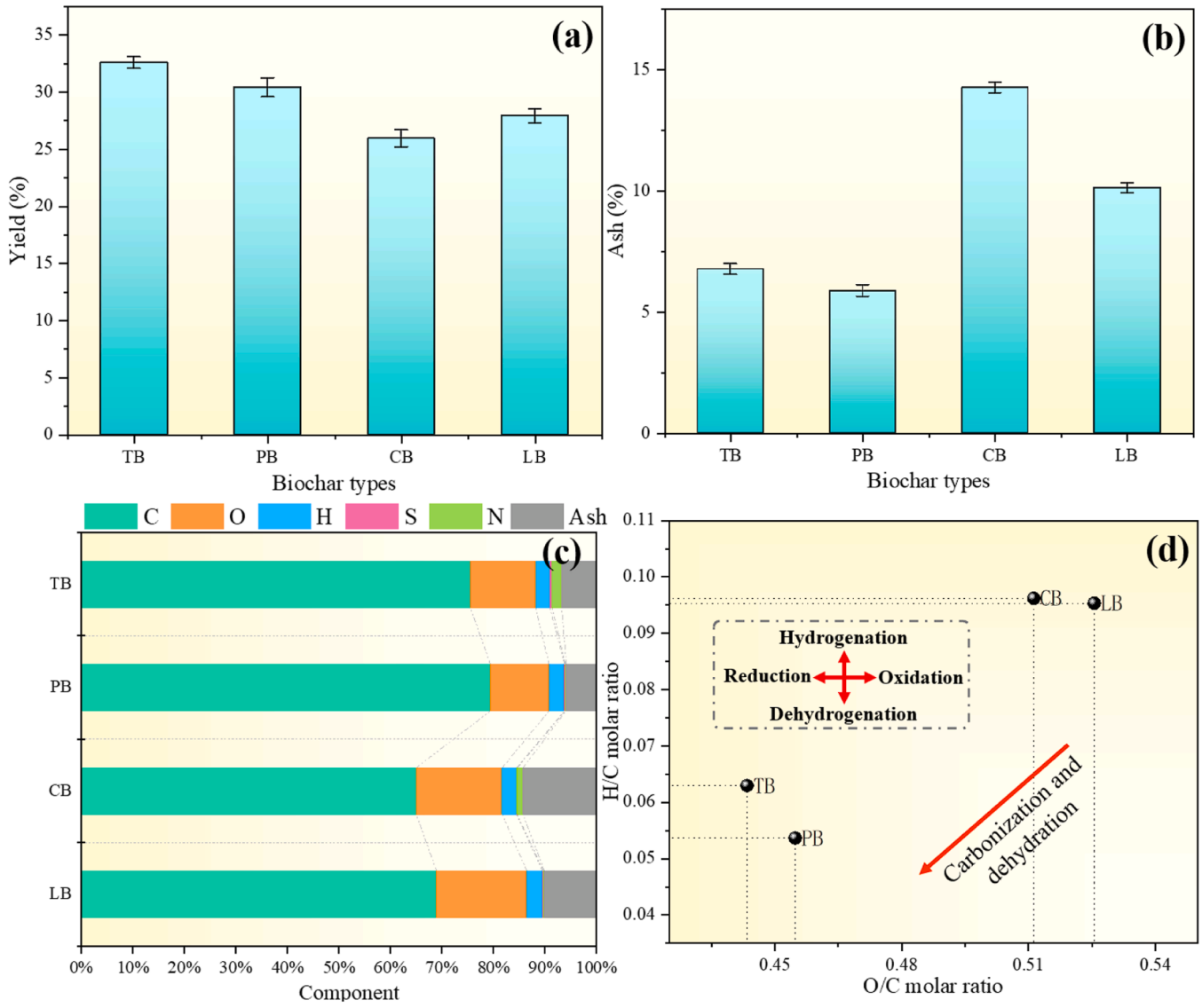

Fig. 8. Biochar characteristics derived from different biomass feedstocks. (a) Biochar yield; (b) Ash content; (c) Elemental composition; (d) Van Krevelen diagram.

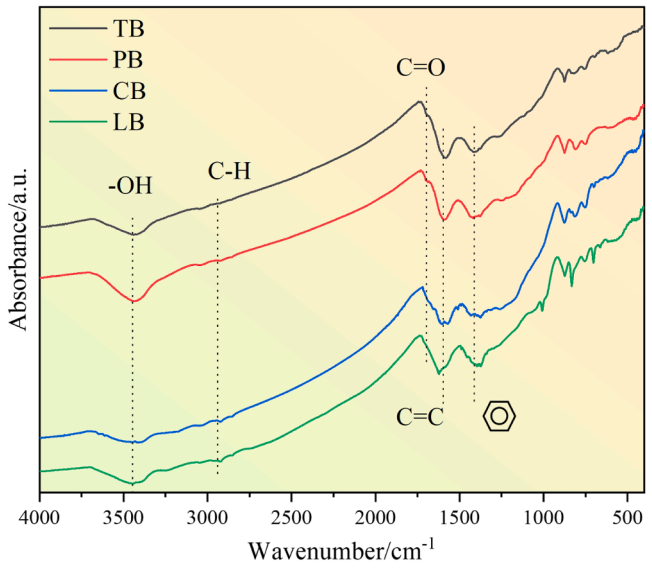

Fig. 9. FTIR spectrum of biochar derived from different biomass.

during high-temperature pyrolysis. The sharp peak at 1700 cm^{-1} corresponds to the stretching vibrations of carbonyl (C═O) groups, while the absorption band at 1540 cm^{-1} is attributed to C═C stretching within aromatic rings. Biochar derived from cellulose-rich biomass exhibited reduced intensities of hydroxyl and methyl/methylene peaks after pyrolysis compared to lignin-rich biochar. This trend can be attributed to the structural nature of cellulose, which, as a linear polysaccharide, underwent more extensive thermal decomposition. As a result, the aliphatic functional groups were more readily volatilized, leading to diminished peak intensities in the corresponding spectral regions. In contrast, lignin-rich biochar retained strong absorption features between 1680–1440 cm^{-1} , indicative of the benzene ring skeletal vibrations. This observation is consistent with the highly aromatic nature of lignin, which is composed of interconnected phenylpropane units forming a robust three-dimensional network.

During pyrolysis, lignin undergoes condensation and polymerization reactions that promote the formation of polyaromatic, graphitic domains, as reflected by the persistence of sharp aromatic peaks. These conjugated π-electron systems enhance structural stability and promote graphitization, which is advantageous for long-term durability, electrical conductivity, and adsorption of small nonpolar molecules [41]. By contrast, the oxygenated functional groups remaining in cellulose-rich

biochar (e.g., residual hydroxyls and carbonyls) are more polar and chemically active, which may favor interactions with polar VOCs or acidic gases. Taken together, these FTIR results highlight a fundamental compositional trade-off: lignin- rich biochar tend to be more aromatic, condensed, and structurally stable, whereas cellulose- rich biochar retain more polar oxygen-containing functionalities. This distinction is crucial for their role in asphalt fume control, as it suggests that lignin-rich biochar may provide a stable framework with high carbon retention, while cellulose-rich biochar contribute active surface groups that enhance adsorption selectivity for specific pollutants.

3.2. Fume emission characteristics of biochar modified asphalt

3.2.1. Thermal evaporation loss of asphalt

The effect of biochar on the thermal evaporation loss of asphalt is shown in Fig. 10. The results indicated that biochar modification significantly reduced thermal evaporation loss of asphalt, with this effect becoming more pronounced as biochar content increased. When the biochar content was 0.25 %, the differences among biochar-modified asphalts were minimal. However, as the biochar dosage increased, the thermal stability differences between different types of biochar became more evident. Lignin-derived biochar (TBA and PBA) consistently exhibited lower evaporation losses than cellulose-derived biochar (CBA and LBA). This superior performance can be attributed to the highly aromatic, condensed carbon structure of lignin-rich biochar, which promotes stronger interfacial interactions with asphalt molecules. Mechanistically, π–π stacking between aromatic rings and hydrogen bonding with polar components enhance the binding of light fractions, thereby restricting their migration under heating. In contrast, cellulose-rich biochar possesses a looser, macropore-dominated structure, which facilitates the diffusion and escape of smaller asphalt molecules. As a result, higher evaporation losses were observed in CBA and LBA. When the biochar content reached 1 %, the evaporation loss of TBA was −0.27 %, while that of CBA is −0.37 %, demonstrating the advantage of lignin-rich biochar in enhancing thermal stability of asphalt. This trend aligns with previous research findings, which have reported that biochar derived from lignin-rich precursors enhances the thermal stability and oxidation resistance of materials [42].

3.2.2. VOCs, H_2S, SO_2, NO_x content in the fumes of BA

The effect of biochar dosage on the emissions of harmful asphalt fumes, including volatile organic compounds (VOCs), hydrogen sulfide (H_2S), sulfur dioxide (SO_2), and nitrogen oxides (NO_x), is shown in Fig. 11. The base asphalt without biochar exhibited extremely high pollutant emissions, with VOCs concentrations reaching 1421 ppm, H_2S levels reaching the instrument detection limit (200 ppm), and SO_2 and NO_x concentrations at 23 ppm and 231 ppm, respectively. The addition of biochar significantly reduced these emissions, with inhibition efficiency increasing as biochar dosage increased.

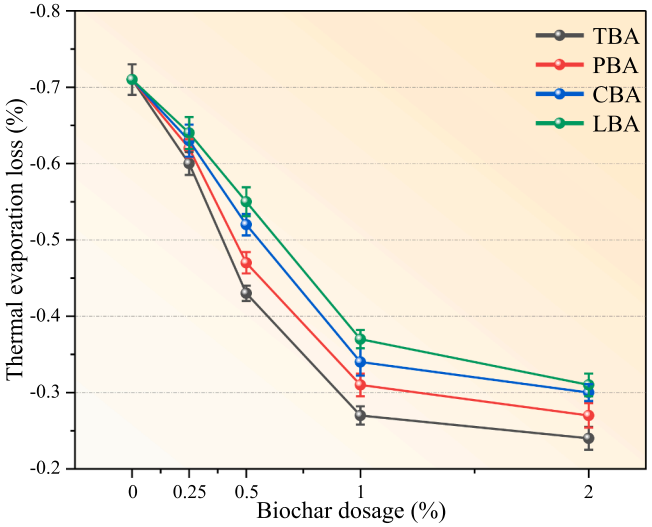

Fig. 10. Effect of biochar on asphalt evaporation loss.

Among the tested biochar, TB demonstrated the most effective VOCs reduction, achieving the lowest residual VOCs levels at higher dosages, followed by PB. In contrast, cellulose-based biochar LB and CB exhibited lower efficiency in VOCs adsorption. At the same dosage, cellulose-rich biochar-modified asphalts retained higher VOCs concentrations compared to lignin-rich biochar. This can be attributed to the higher specific surface area and abundant microporous structure of lignin-rich biochar, as revealed by BET and SEM analyses, which provide numerous physical adsorption sites for capturing nonpolar volatile compounds. The addition of biochar also effectively suppressed H_2S emissions. At lower dosages, cellulose-based biochar showed higher removal efficiency than lignin-based biochar. However, as the dosage increased (above 1 %), all biochar reached similar H_2S inhibition levels, suggesting adsorption saturation at higher dosages. This superior performance likely stems from their higher abundance of oxygen-containing functional groups, as confirmed by FTIR spectra, which promote stronger interactions with polar gases. The reduction trend in NO_x emissions followed a similar pattern, with CB and LB outperforming TB and PB, reflecting their superior ability to adsorb polar gases. However, at higher dosages, the performance differences among the biochar became less pronounced. In contrast, SO_2 suppression showed the least variation among the different biochar types. When the biochar dosage exceeded 1 %, SO_2 was almost completely removed by all materials.

Overall, these results highlight a distinct division of adsorption roles between lignin-rich and cellulose-rich biochar: the former, with their condensed aromatic structures and microporous networks, are more effective in reducing VOCs; the latter, enriched in oxygenated functional groups, are better suited for polar gases such as H_2S and NO_x. At higher dosages, these differences diminish, indicating that biochar application at sufficient loading can provide a comprehensive suppression of multiple asphalt fume components.

3.2.3. Concentration of various components in asphalt fume

The chemical composition of VOCs emitted from base asphalt and 1 % biochar-modified asphalt was analyzed using gas chromatography-mass spectrometry (GC-MS), as shown in Fig. 12. Each chromatographic peak corresponds to a specific compound, and qualitative identification was performed by matching mass spectra with reference databases. The peak intensity, which is positively correlated with the compound concentration, was used for quantitative analysis. Notably, biochar modification significantly suppressed the release of VOCs, as evidenced by the reduction in characteristic peak intensities across all biochar-modified asphalt samples compared to the base asphalt.

To systematically evaluate the composition of VOCs, the detected compounds were classified into four major categories based on their chemical structures: aliphatic hydrocarbons (AH), aromatic compounds (AC), oxygen-containing compounds (OC), and sulfur-containing compounds (SC) (Fig. 13). The base asphalt exhibited a diverse distribution of VOCs, with a total of 91 different compounds identified. The majority consisted of AH (42.87 %) and AC (53.28 %), while OC (2.68 %) and SC (1.18 %) contributed minimally.

The introduction of biochar significantly reduced both the diversity and concentration of VOCs, with lignin-rich biochar (TB and PB) exhibiting higher inhibition efficiency compared to cellulose-rich biochar (CB and LB). In the base asphalt fume composition, 58 AH compounds and 23 AC compounds were detected, along with 6 OC and 4 SC compounds (Fig. 13a). Biochar modification significantly decreased the number of VOCs species, with lignin-rich biochar demonstrating superior inhibition efficiency compared to cellulose-rich biochar. Specifically: 1TBA reduced the total number of VOCs by 29 species (AH: −20, AC: −6, OC: −1, SC: −2), lowering the total VOCs concentration to

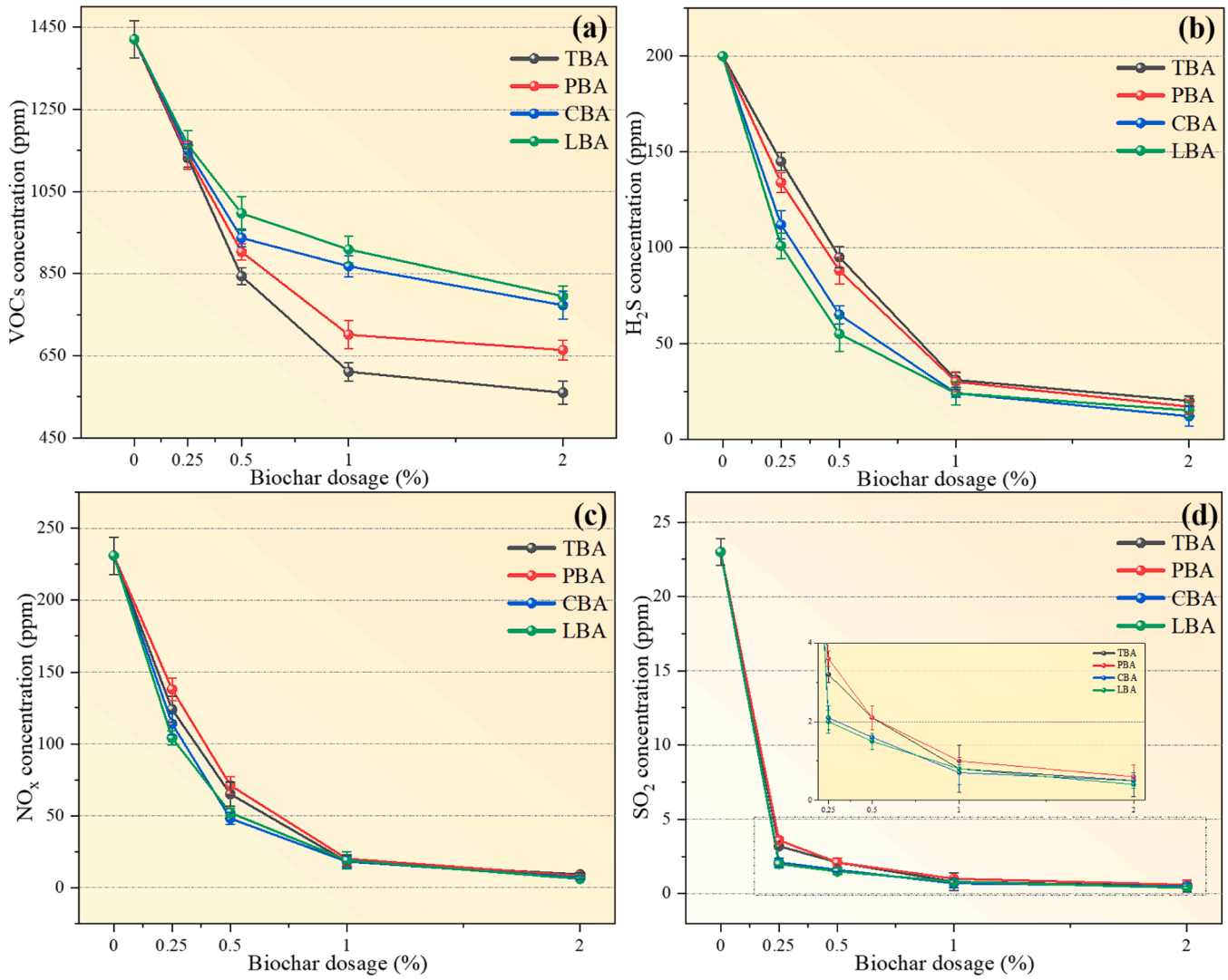

Fig. 11. Effect of biochar on asphalt fume: (a) VOCs; (b) H_2S; (c) NO_x; (d) SO_2.

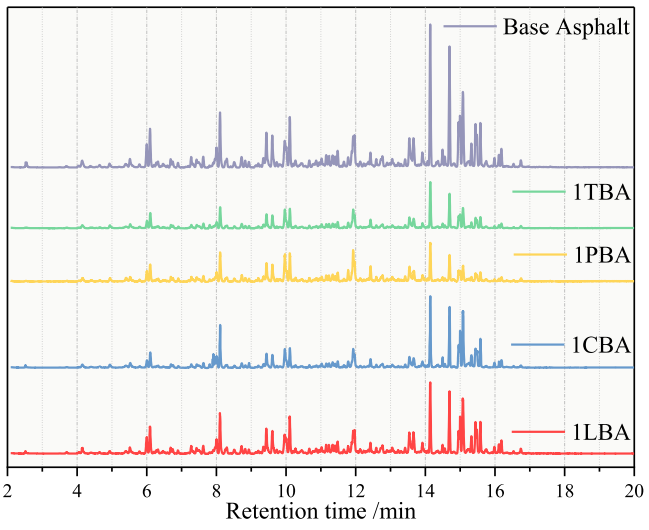

Fig. 12. GC-MS results of base asphalt and TB-A.

33.72 % of the base asphalt level. 1PBA reduced VOCs by 25 species (AH: −18, AC: −6, OC: −2, SC: −2), leaving a residual concentration of 49.99 %. 1CBA and 1LBA exhibited smaller reductions: 1CBA: 19 fewer VOC species (AH: −13, AC: −2, OC: −3, SC: −3), 1LBA: 17 fewer VOC species (AH: −11, AC: −3, OC: −3, SC: −2).

The observed differences in inhibition efficiency of VOCs can be attributed to the distinct physicochemical properties of lignin- and cellulose-rich biochar. Their hierarchical porosity enables a dual adsorption mechanism: mesopores and macropores facilitate the diffusion of asphalt fume molecules, while micropores act as primary adsorption sites, effectively capturing small VOCs molecules. Additionally, its highly aromatic and condensed carbon structure enhances π–π interactions with polycyclic aromatic hydrocarbons (PAHs) in asphalt fumes, leading to superior adsorption of AC compounds. In contrast, cellulose-rich biochar features a more open macropores structure, which reduces the physical confinement for fume molecules, thereby lowering its effectiveness in VOCs capture. However, cellulose-rich biochar exhibited better adsorption of OC and SC compounds, likely due to their higher content of oxygen-containing functional groups, making them more suitable for removing polar pollutants.

These results demonstrate that the adsorption capacity of biochar is governed by a combination of surface area, pore size distribution, and surface functionalization. The significantly higher VOCs suppression efficiency of lignin-rich biochar suggests its potential as effective

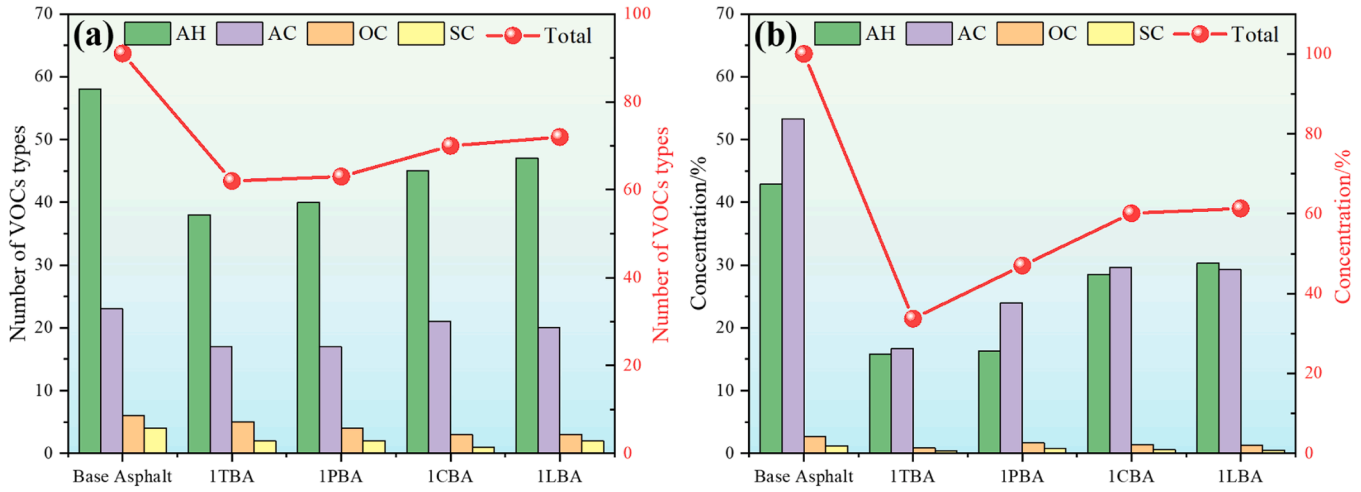

Fig. 13. Influence of TB on the number of VOCs types in asphalt fume.

modifiers for asphalt emissions control.

3.2.4. *Effect of biochar on SARA fractions of asphalt*

The effect of biochar on the fraction of asphalt saturates, aromatics, resins, and asphaltenes (SARA fractions) is shown in Fig. 14. The results indicated that biochar modification altered the distribution of asphalt fractions to some extent, depending on the type of biochar used. As shown in the figure, lignin-rich biochar had a relatively minor impact on asphalt composition, whereas cellulose-rich biochar induced more pronounced changes. A consistent trend across all biochar-modified asphalt samples was the increase in asphaltene content. This effect can be attributed to the insolubility of both biochar and asphaltenes, which promotes preferential interactions and phase separation, leading to the apparent enrichment of asphaltenes. At the same time, the proportions of saturates and aromatics decreased, while the resin fraction increased. This redistribution suggests that biochar acts as both an adsorbent and a catalytic interface, facilitating the transformation of lighter asphalt fractions into heavier and more stable components. Such a conversion is likely driven by adsorption of low-molecular-weight species onto biochar surfaces, followed by molecular condensation or immobilization at active sites. Mechanistic differences between lignin- and cellulose-rich biochar further explain the observed variations. Lignin-rich biochars, with their condensed aromatic carbon structures, are relatively inert and thermally stable, thus engaging mainly in physical adsorption processes.

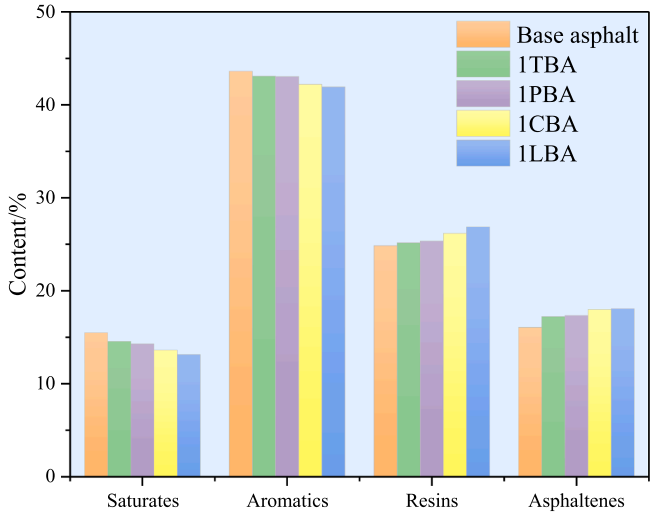

Fig. 14. Effect of biochar on SARA components of asphalt.

Consequently, their impact on SARA distribution remains limited. By contrast, cellulose-rich biochars contain abundant oxygen-containing functional groups (e.g., hydroxyl, carboxyl, and carbonyl groups), which can interact with polar asphalt components through hydrogen bonding or dipole–dipole interactions. These chemical interactions promote the conversion of lighter fractions into resin-like structures, thereby amplifying changes in asphalt composition.

3.3. *Physical properties of biochar modified asphalt*

The influence of biochar modification on the physical properties of asphalt, including penetration, ductility, softening point, and viscosity, is presented in Fig. 15. The results indicated that biochar incorporation significantly alters the physical characteristics of asphalt, with variations based on biochar type and dosage. Moreover, a statistical comparison was conducted on the effects of biochar on the physical properties of asphalt at each dosage level. The resulting p-values and significance levels are provided in Tables S1-S4.

As shown in Fig. 15a, the penetration of asphalt gradually decreased with increasing biochar content, indicating that biochar enhanced the structural stiffness of asphalt. This effect was more pronounced for cellulose-rich biochar, where the penetration of CBA and LBA dropped below 60 dmm (1 dmm = 0.1 mm) at a 2 % biochar content, suggesting a modification in asphalt gradation. The reduction in penetration can be attributed to the increase in asphaltene content caused by biochar addition, which strengthens the rigid phase of asphalt and reduces the mobility of lighter fractions. Meanwhile, the softening point of biochar-modified asphalt increased with rising biochar content, demonstrating improved resistance to high-temperature deformation. Cellulose-rich biochars produced the most pronounced increases in softening point, likely due to their larger pore structures and higher affinity for light asphalt components. These features enhance molecular interactions at the biochar–asphalt interface, thereby reducing thermal sensitivity. This finding highlights the potential of cellulose-rich biochars for improving asphalt performance in hot climates where rutting resistance is critical.

As biochar content increased, the ductility of the asphalt decreased, indicating reduced low-temperature crack resistance. At low biochar dosages (≤0.5 %), the impact on ductility was minimal. However, when the biochar content reached 1 %, a sharp decline in ductility was observed, particularly in cellulose-rich biochar samples, where reductions of 31 % (CBA), 29 % (LBA), 24 % (PBA), and 22 % (TBA) were recorded compared to the base asphalt. At a 2 % biochar dosage, ductility further decreased by 50 % (CBA), 48 % (LBA), 41 % (PBA), and 37 % (TBA). This reduction in ductility can be attributed to several factors. First, the incorporation of biochar alters the colloidal

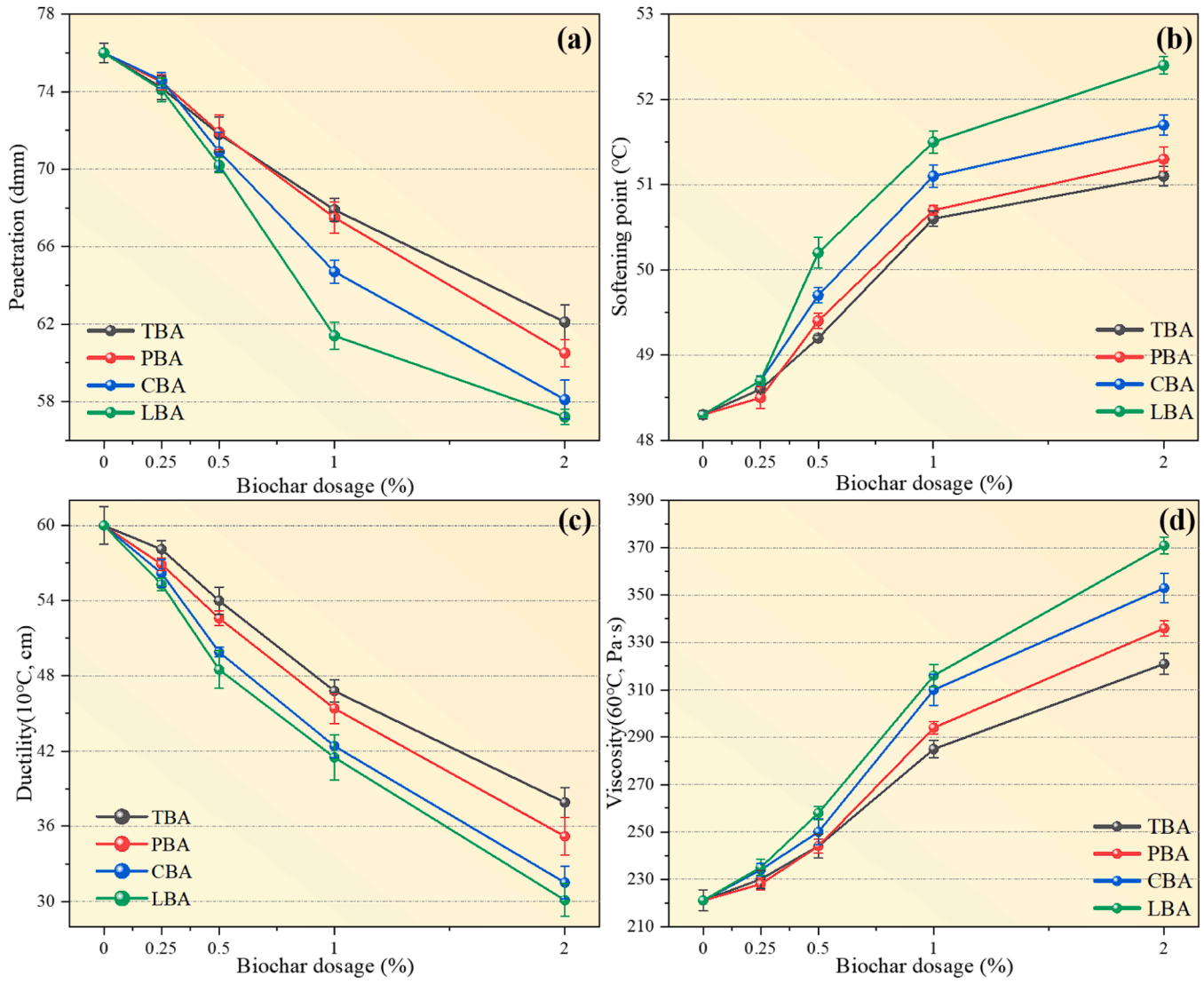

Fig. 15. Physical properties of different biochar modified asphalt: (a) Penetration; (b) Softening point; (c) Ductility; (d) Viscosity.

equilibrium of asphalt by increasing the proportion of heavy fractions, thereby reducing its flexibility. Second, biochar particles act as rigid inclusions within the asphalt matrix, disrupting the continuity of the colloidal network and leading to localized stress concentrations. At higher dosages, the limited mobility of asphalt components around biochar particles exacerbates this effect, resulting in brittle failure under tensile stress. However, this deterioration trend can be attenuated to some extent by selecting lignin-rich biochar at low dosage, and thus optimized biochar selection and dosage adjustment can mitigate the extent of ductility reduction.

The viscosity of the bitumen increased with the addition of biochar. This increase is mainly due to the ability of biochar to adsorb light components from asphalt, which leads to the transition of asphalt from a sol-gel to a gel-type colloidal structure, while the macropores structure of cellulose-rich biochar has a greater ability to adsorb light components of asphalt than the lignin-rich biochar, and thus the viscosity value of CBA is always slightly higher. In addition, biochar acts as a reinforcing skeleton in the asphalt matrix, restricting molecular flow, which also contributes to the increase in viscosity.

The primary objective of incorporating biochar into asphalt is to suppress fume emissions as much as possible without compromising service performance. While the addition of biochar enhances the high-temperature properties of asphalt, it may also lead to some reduction in low-temperature flexibility. For regions where low-temperature performance is critical, such as cold or severe climates, a 0.5 % dosage of biochar-modified asphalt is recommended. In high-temperature regions, where moderate reductions in ductility are generally acceptable, higher dosages can be considered. For general applications without strict temperature requirements, a 1 % dosage offers an optimal balance. This level not only ensures effective fume suppression but also minimizes adverse impacts on low-temperature ductility. Among the tested materials, TB and PB samples in particular demonstrate satisfactory performance across most application scenarios.

4. Conclusions

This study elucidates how the lignin and cellulose controls the structural and compositional characteristics of biochar and analyzes the relationship between these characteristics and its ability to suppress asphalt fumes. The main conclusions are as follows:

1. BET, SEM, and FTIR analyses confirmed that biomass composition dictates biochar properties. Lignin-rich biochar (TB, PB) formed micropore- and mesopore-dominated structures with higher surface area and aromaticity, reflecting greater carbonization and stability. In contrast, cellulose-rich biochar (CB, LB) developed macroporous

structures with lower surface areas but retained more oxygen-containing functional groups, imparting higher polarity.
2. Lignin-rich feedstocks produced higher biochar yields with lower ash due to thermal stability, while cellulose-rich materials decomposed more and accumulated inorganic residues. Elemental and Van Krevelen analyses showed lignin-derived biochar was richer in carbon and hydrogen, whereas cellulose-derived biochar preserved more oxygenated groups, aligning with FTIR results.
3. Biochar reduced asphalt volatilization, with lignin-rich biochar showing superior performance by stabilizing light fractions through π–π interactions and hydrogen bonding. Cellulose-rich biochar, due to macroporous networks, allowed greater migration of volatile components, resulting in higher evaporation losses.
4. Real-time monitoring and GC-MS demonstrated that biochar effectively suppressed asphalt fumes. Lignin-derived biochar most effectively adsorbed VOCs and aromatic hydrocarbons via micropores and π–π interactions, while cellulose-derived biochar preferentially removed polar gases (H_2S, NO_x) due to abundant oxygen functionalities. All biochar types nearly eliminated SO_2 emissions at dosages above 1 %.
5. Biochar addition promoted conversion of light fractions to resins and asphaltenes, enhancing high-temperature performance but reducing ductility at higher dosages. Cellulose-derived biochar caused greater compositional changes and stiffness, while lignin-derived biochar offered a more balanced effect. An optimal dosage of 1 % achieved effective fume suppression with minimal negative impact on service performance. For cold regions, lower dosages (0.25–0.5 %) may be more appropriate, whereas higher dosages (≥1.5 %) could be considered in hot climates where rutting resistance is critical.

Recommendations for future work

This study investigated the effects of biochar derived from cellulose-rich and lignin-rich biomass pyrolysis on asphalt fume emissions and examined its impact on the physical properties of asphalt. Future research should focus on optimizing biochar surface functionalization to improve compatibility with asphalt components, thereby minimizing adverse effects on low-temperature performance. Additionally, aging studies should be conducted to assess the durability and oxidative stability of biochar-modified asphalt in practical applications.

CRediT authorship contribution statement

Hao Duan: Writing – review & editing, Writing – original draft. **Quantao Liu:** Methodology, Investigation. **Yanheng He:** Visualization, Validation. **Zizhou Shen:** Visualization, Validation. **Xiaobin Han:** Visualization, Validation. **Shi Xu:** Visualization, Validation. **Jianying Yu:** Resources, Project administration, Methodology.

Declaration of Competing Interest

The authors declare that they have no known competing financial interests or personal relationships that could have appeared to influence the work reported in this paper.

Acknowledgement

This work was supported by the Science and Technology Project of Petro China Co. Ltd (RLY-2023Y-03) and State Key Laboratory of Silicate Materials for Architectures (Wuhan University of Technology) (SYSJJ2024–19).

Appendix A. Supporting information

Supplementary data associated with this article can be found in the online version at doi:10.1016/j.conbuildmat.2025.143655.

Data availability

Data will be made available on request.

References

[1] D. Lu, X. Jiang, Z. Tan, B. Yin, Z. Leng, J. Zhong, Enhancing sustainability in pavement engineering: a-state-of-the-art review of cement asphalt emulsion mixtures, Clean. Mater. 9 (2023) 100204, https://doi.org/10.1016/j.clema.2023.100204.
[2] M. Hoy, V. Samrandee, W. Samrandee, A. Suddeepong, I. Phummiphan, S. Horpibulsuk, A. Buritatum, A. Arulrajah, C. Yeanyong, Evaluation of asphalt pavement maintenance using recycled asphalt pavement with asphalt binders, Constr. Build. Mater. 406 (2023) 133425, https://doi.org/10.1016/j.conbuildmat.2023.133425.
[3] X. Jiang, H. Zhu, Z. Yan, F. Zhang, X. Huang, Z. Leng, C. Yan, N. Hua, D. Lu, X. Zhang, R. Xiao, Fire-Retarding asphalt pavement for urban road tunnels: a state-of-the-art review and beyond, Fire Technol. (2024), https://doi.org/10.1007/s10694-024-01556-2.
[4] D. Jiang, Z. Cao, G. Gong, C. Wang, Y. Gao, VOCs inhibited asphalt mixtures for green pavement: emission reduction behavior, environmental health impact and road performance, J. Clean. Prod. 489 (2025) 144671, https://doi.org/10.1016/j.jclepro.2025.144671.
[5] J. Zhang, M. Chen, B. Leng, S. Wu, D. Chen, Z. Zhao, Investigation on storage stability, H2S emission and rheological properties of modified asphalt with different pretreated waste rubber powder, J. Clean. Prod. 456 (2024) 142469, https://doi.org/10.1016/j.jclepro.2024.142469.
[6] S. Mo, Y. Wang, F. Xiong, C. Ai, Effects of asphalt source and mixing temperature on the generated asphalt fumes, J. Hazard. Mater. 371 (2019) 342–351, https://doi.org/10.1016/j.jhazmat.2019.03.025.
[7] S. Zeng, S. Mao, S. Xu, Y. He, J. Yu, Investigation on DOPO as reactive fumes suppressant to reduce the fumes emission of asphalt, J. Hazard. Mater. 463 (2024) 132878, https://doi.org/10.1016/j.jhazmat.2023.132878.
[8] Y. Lv, S. Wu, N. Li, Q. Liu, C. Yang, Y. Zou, S. Amirkhanian, Flue gas suppression and environmental evaluation of deodorizer-modified rubber asphalt based on radar method, Constr. Build. Mater. 411 (2024) 134526, https://doi.org/10.1016/j.conbuildmat.2023.134526.
[9] M. Neghab, F.Z. Derisi, J. Hassanzadeh, V. Dirin, S. Heidari, Toxic responses of different organs following occupational exposure to sub-threshold limit value levels of paving asphalt fumes, Toxicol. Environ. Chem. 99 (2016) 331–339, https://doi.org/10.1080/02772248.2016.1172581.
[10] Y. Xiao, M. Wan, K.J. Jenkins, S.P. Wu, P.Q. Cui, Using activated carbon to reduce the volatile organic compounds from bituminous materials, J. Mater. Civ. Eng. 29 (2017) 04017166, https://doi.org/10.1061/(ASCE)MT.1943-5533.0002024.
[11] S. Li, Q. Liu, H. Wang, J. Wang, L. He, S. Wu, Effect of kaolin and sepiolite on fume emissions of rubber modified asphalt, Constr. Build. Mater. 416 (2024) 135276, https://doi.org/10.1016/j.conbuildmat.2024.135276.
[12] X. Yang, A. Shen, Y. Su, W. Zhao, Effects of alumina trihydrate (ATH) and organic montmorillonite (OMMT) on asphalt fume emission and flame retardancy properties of SBS-modified asphalt, Constr. Build. Mater. 236 (2020) 117576, https://doi.org/10.1016/j.conbuildmat.2019.117576.
[13] X. Zhang, Y. Xiao, Y. Long, Z. Chen, P. Cui, R. Wu, X. Chang, VOCs reduction in bitumen binder with optimally designed Ca(OH)2-incorporated zeolite, Constr. Build. Mater. 279 (2021) 122485, https://doi.org/10.1016/j.conbuildmat.2021.122485.
[14] X. Chang, L. Wan, Y. Long, Y. Xiao, Y. Xue, Optimal zeolite structure design for VOC emission reduction in asphalt materials, Constr. Build. Mater. 366 (2023) 130227, https://doi.org/10.1016/j.conbuildmat.2022.130227.
[15] Y. Lv, S. Wu, N. Li, P. Cui, H. Wang, S. Amirkhanian, Z. Zhao, Performance and VOCs emission inhibition of environmentally friendly rubber modified asphalt with UiO-66 MOFs, J. Clean. Prod. 385 (2023) 135633, https://doi.org/10.1016/j.jclepro.2022.135633.
[16] M. Lin, F. Li, X. Li, X. Rong, K. OH, Biochar-clay, biochar-microorganism and biochar-enzyme composites for environmental remediation: a review, Environ. Chem. Lett. 21 (2023) 1837–1862, https://doi.org/10.1007/s10311-023-01582-6.
[17] Y. Yi, Z. Huang, B. Lu, J. Xian, E.P. Tsang, W. Cheng, J. Fang, Z. Fang, Magnetic biochar for environmental remediation: a review, Bioresour. Technol. 298 (2020) 122468, https://doi.org/10.1016/j.biortech.2019.122468.
[18] G. Ravindiran, S. Rajamanickam, G. Janardhan, G. Hayder, A. Alagumalai, O. Mahian, S.S. Lam, C. Sonne, Production and modifications of biochar to engineered materials and its application for environmental sustainability: a review, Biochar 6 (2024) 62, https://doi.org/10.1007/s42773-024-00350-1.
[19] Effects of using biochar materials obtained from cherry and sour cherry wastes on bitumen modification, Construction and Building Materials 489 (2025) 140609. https://doi.org/10.1016/j.conbuildmat.2025.140609.
[20] C. Celauro, R. Teresi, N.T. Dintcheva, Evaluation of anti-aging effect in biochar-modified bitumen, Sustainability 15 (2023) 10583, https://doi.org/10.3390/su151310583.
[21] Enhancing Biomass Value Chain by Utilizing Biochar as A Free Radical Scavenger to Delay Ultraviolet Aging of Bituminous Composites Used in Outdoor Construction, Resour. Conserv. Recycl. 168 (2021) 105302. https://doi.org/10.1016/j.resconrec.2020.105302.
[22] M. Ji, X. Wang, M. Usman, F. Liu, Y. Dan, L. Zhou, S. Campanaro, G. Luo, W. Sang, Effects of different feedstocks-based biochar on soil remediation: a review,

Environ. Pollut. 294 (2022) 118655, https://doi.org/10.1016/j.envpol.2021.118655.
[23] H. Yang, S. Ye, Z. Zeng, G. Zeng, X. Tan, R. Xiao, J. Wang, B. Song, L. Du, M. Qin, Y. Yang, F. Xu, Utilization of biochar for resource recovery from water: a review, Chem. Eng. J. 397 (2020) 125502, https://doi.org/10.1016/j.cej.2020.125502.
[24] H. Zhu, Q. An, A. Syafika Mohd Nasir, A. Babin, S. Lucero Saucedo, A. Vallenas, L. Li, S.A. Baldwin, A. Lau, X. Bi, Emerging applications of biochar: a review on techno-environmental-economic aspects, Bioresour. Technol. 388 (2023) 129745, https://doi.org/10.1016/j.biortech.2023.129745.
[25] M. Mousavi, S. Aldagari, E.H. Fini, Adsorbing volatile organic compounds within bitumen improves colloidal stability and air quality, ACS Sustain. Chem. Eng. 11 (2023) 9581–9594, https://doi.org/10.1021/acssuschemeng.3c00539.
[26] Y. Zhou, C. Shen, T. Wang, Y. Xue, Inhibition effect of three types of biochar on volatile organic compounds from asphalt: revealing chemical adsorption as the primary mechanism, Constr. Build. Mater. 411 (2024) 134322, https://doi.org/10.1016/j.conbuildmat.2023.134322.
[27] N.K. Gupta, P. Prakash, P. Kalaichelvi, K.N. Sheeba, The effect of temperature and hemicellulose-lignin, cellulose-lignin, and cellulose-hemicellulose on char yield from the slow pyrolysis of rice husk, Energy Sources Part A 38 (2016) 1428–1434, https://doi.org/10.1080/15567036.2014.941518.
[28] L. Reyes, L. Abdelouahed, C. Mohabeer, J.-C. Buvat, B. Taouk, Energetic and exergetic study of the pyrolysis of lignocellulosic biomasses, cellulose, hemicellulose and lignin, Energy Convers. Manag. 244 (2021) 114459, https://doi.org/10.1016/j.enconman.2021.114459.
[29] N.A. Baharum, H.M. Nasir, M.Y. Ishak, N.M. Isa, M.A. Hassan, A.Z. Aris, Highly efficient removal of diazinon pesticide from aqueous solutions by using coconut shell-modified biochar, Arab. J. Chem. 13 (2020) 6106–6121, https://doi.org/10.1016/j.arabjc.2020.05.011.
[30] W. Xue, F. Zhang, W. Ding, K. Zhang, Q. Zhang, Enhanced removal of fluoride ions using lanthanum-doped coconut shell biochar in PVDF ultrafiltration membranes, J. Hazard. Mater. 480 (2024) 136393, https://doi.org/10.1016/j.jhazmat.2024.136393.
[31] S. Shan, H. Wu, J. Yang, D. Jiao, M. Huang, F. Li, Effective removal of phenol from wastewater by magnetic porous loofah biochar, Carbon Lett. 34 (2023) 191–200, https://doi.org/10.1007/s42823-023-00662-5.
[32] Z. Hao, Q. Wang, Z. Yan, H. Jiang, Novel magnetic loofah sponge biochar enhancing microbial responses for the remediation of polycyclic aromatic hydrocarbons-contaminated sediment, J. Hazard. Mater. 401 (2021) 123859, https://doi.org/10.1016/j.jhazmat.2020.123859.
[33] F. Lin, L. Wang, X. Dai, Z. Man, Y. Meng, D. Chu, Y. Yang, W. Wang, H. Xiao, K. Wang, Catalytic fixation of hydrogen sulfide over CuO-CaCO3 co-impregnated tea stalk-derived biochar, J. Environ. Chem. Eng. 12 (2024) 113320, https://doi.org/10.1016/j.jece.2024.113320.
[34] S. Cheng, Y. Liu, B. Xing, X. Qin, C. Zhang, H. Xia, Lead and cadmium clean removal from wastewater by sustainable biochar derived from poplar saw dust, J. Clean. Prod. 314 (2021) 128074, https://doi.org/10.1016/j.jclepro.2021.128074.
[35] Y. Mao, B. Cai, M. Huang, X. Liu, W. Zhang, Z. Ma, A sustainable preparation strategy for the nitrogen-doped hierarchical biochar with high surface area for the enhanced removal of organic dye, Biochar 5 (2023) 70, https://doi.org/10.1007/s42773-023-00269-z.
[36] S. Wei, M. Zhu, X. Fan, J. Song, P. Peng, K. Li, W. Jia, H. Song, Influence of pyrolysis temperature and feedstock on carbon fractions of biochar produced from pyrolysis of rice straw, pine wood, pig manure and sewage sludge, Chemosphere 218 (2019) 624–631, https://doi.org/10.1016/j.chemosphere.2018.11.177.
[37] H. Duan, Q. Liu, S. Mao, Y. He, X. Han, J. Yu, S. Xu, Effect of tea stalk biochar derived from pyrolysis at different temperatures on adsorption capacity of asphalt fume, Constr. Build. Mater. 481 (2025) 141523, https://doi.org/10.1016/j.conbuildmat.2025.141523.
[38] Z. Deller, F. Giustozzi, S. Maniam, Predicting odorous emissions from bitumen collected at 13 refineries: a combined GC–MS and supervised learning approach, Fuel 364 (2024) 131142, https://doi.org/10.1016/j.fuel.2024.131142.
[39] M.O. Akca, P.A. Bozkurt, F. Gokmen, H. Akca, K.D. Yağcıoğlu, V. Uygur, Engineering the biochar surfaces through feedstock variations and pyrolysis temperatures, Ind. Crops Prod. 218 (2024) 118819, https://doi.org/10.1016/j.indcrop.2024.118819.
[40] E. Ranzi, P.E.A. Debiagi, A. Frassoldati, Mathematical modeling of fast biomass pyrolysis and Bio-Oil formation. Note I: kinetic mechanism of biomass pyrolysis, ACS Sustain. Chem. Eng. 5 (2017) 2867–2881, https://doi.org/10.1021/acssuschemeng.6b03096.
[41] C. Chen, K. Sun, C. Huang, M. Yang, M. Fan, A. Wang, G. Zhang, B. Li, J. Jiang, W. Xu, J. Liu, Investigation on the mechanism of structural reconstruction of biochars derived from lignin and cellulose during graphitization under high temperature, Biochar 5 (2023) 51, https://doi.org/10.1007/s42773-023-00229-7.
[42] F. Li, X. Gui, W. Ji, C. Zhou, Effect of calcium dihydrogen phosphate addition on carbon retention and stability of biochars derived from cellulose, hemicellulose, and lignin, Chemosphere 251 (2020) 126335, https://doi.org/10.1016/j.chemosphere.2020.126335.